nature chemistry

ARTICLES

PUBLISHED ONLINE: 13 JULY 2014 | DOI: 10.1038/NCHEM.1999

Observation of an all-boron fullerene

Hua-Jin Zhai[1], Ya-Fan Zhao[2], Wei-Li Li[3], Qiang Chen[1], Hui Bai[1], Han-Shi Hu[2], Zachary A. Piazza[3], Wen-Juan Tian[1], Hai-Gang Lu[1], Yan-Bo Wu[1], Yue-Wen Mu[1], Guang-Feng Wei[4], Zhi-Pan Liu[4], Jun Li[2]*, Si-Dian Li[1]* and Lai-Sheng Wang[3]*

After the discovery of fullerene-C_{60}, it took almost two decades for the possibility of boron-based fullerene structures to be considered. So far, there has been no experimental evidence for these nanostructures, in spite of the progress made in theoretical investigations of their structure and bonding. Here we report the observation, by photoelectron spectroscopy, of an all-boron fullerene-like cage cluster at B_{40}^- with an extremely low electron-binding energy. Theoretical calculations show that this arises from a cage structure with a large energy gap, but that a quasi-planar isomer of B_{40}^- with two adjacent hexagonal holes is slightly more stable than the fullerene structure. In contrast, for neutral B_{40} the fullerene-like cage is calculated to be the most stable structure. The surface of the all-boron fullerene, bonded uniformly via delocalized σ and π bonds, is not perfectly smooth and exhibits unusual heptagonal faces, in contrast to C_{60} fullerene.

After the discovery of buckminsterfullerene (C_{60})[1], the existence of a similar B_{60} fullerene was not considered for over two decades, mainly because of the electron deficiency of boron. Even with a recent interesting theoretical proposition[2], heretofore there has been no experimental evidence for boron fullerenes. Early mass spectra of boron clusters showed no special abundance of the B_{60} cluster[3]. Over the past decade, joint experimental and theoretical efforts have been used to systematically elucidate the electronic and structural evolution of elemental boron clusters, and have uncovered a new world of flat boron[4–9]. Planar or quasi-planar (2D) boron clusters were shown to be the most-stable structures for anionic B_n^- clusters up to at least $n = 24$, governed by σ and π delocalized bonding[8,10]. Most recently, B_{36}^- was discovered to possess a 2D structure with a perfect hexagonal hole in its centre[11], which suggested that extended 2D atomically thin boron sheets (borophene) might be viable experimentally. Low-dimensional boron nanostructures have also been studied theoretically[12–14]. In particular, the proposal of a B_{80} fullerene[15] spurred renewed interest in all-boron fullerenes[16–23], although further theoretical work showed that core–shell structures are much lower in energy[24–27]. Thus, whether all-boron fullerenes exist or not has remained an open question. Here we report the experimental observation and characterization of an all-boron fullerene cluster at B_{40}^-, along with a 2D isomer. The 2D B_{40}^- with two adjacent hexagonal holes represents the global minimum, whereas the nearly degenerate fullerene-like B_{40}^- cage is slightly higher in energy. However, for neutral B_{40} the fullerene structure is overwhelmingly the global minimum with unprecedented delocalized bonding over the cage surface.

Results

Photoelectron spectra. The B_{40}^- clusters were produced in a laser-vaporization supersonic source and characterized using photoelectron spectroscopy (PES)[28]. The photoelectron spectrum at 193 nm photon energy is shown in Fig. 1a, and the 266 nm spectrum is presented in Supplementary Fig. 1. B_{40}^- distinguishes itself from other boron clusters by its exceptional electronic properties. Its leading spectral band X′ has an extremely low vertical detachment energy (VDE) of 2.62 ± 0.05 eV. The overall spectral pattern is unusually simple for such a large cluster: bands X′, X (VDE, 3.63 ± 0.05 eV) and A (VDE, 4.24 ± 0.03 eV) are well separated, which suggests a remarkably stable neutral B_{40} cluster with a sizable energy gap between its highest occupied molecular orbital (HOMO) and lowest unoccupied molecular orbital (LUMO). Higher binding energy bands are also observed at B (5.10 eV), C (5.55 eV) and D (6.08 eV).

The well-resolved photoelectron spectral features serve as electronic fingerprints, which makes it possible to determine the structure of B_{40}^- by comparison with theoretical calculations, as recently done for B_{36}^- (ref. 11) and for other smaller boron clusters[4–8]. Furthermore, the intensity ratio of bands X′ and X can be varied slightly on changes of the supersonic expansion conditions, which hints that they may originate from coexisting isomers in the B_{40}^- cluster beam. The adiabatic detachment energies (ADEs) for bands X′ and X were evaluated from their onset to be 2.50 ± 0.05 eV and 3.51 ± 0.05 eV, respectively, which represent the electron affinities of their corresponding neutral species. The ADE of the X′ band is exceptionally low in comparison with the already low ADE of B_{36}^- (3.12 eV)[11] and that of B_{24}^- (3.55 eV)[8], which indicates a major structural change at B_{40}^-.

Structural searches. Unbiased global-minimum searches were performed for B_{40}^- and B_{40} using both the stochastic surface walking (SSW)[29] and basin hopping (BH)[30] algorithms. Low-lying structures were then optimized fully and their relative energies were evaluated using three density functional theory (DFT) methods with the 6-311+G* basis set[31]: PBE[32], PBE0[33] and TPSSh[33,34]. Isomers within ~1.5 eV above the global minima are collected in Supplementary Figs 2 and 3 for B_{40}^- and B_{40}, respectively. Relative energies at the PBE0/6-311+G* level should be reliable for the current systems because this level has been tested extensively in prior works and found to be suitable for boron clusters[6–11]. For more accurate relative energies, single-point CCSD (coupled-cluster single-double) calculations with optimized

---

[1]Institute of Molecular Science, Shanxi University, Taiyuan 030006, China, [2]Department of Chemistry & Key Laboratory of Organic Optoelectronics and Molecular Engineering of Ministry of Education, Tsinghua University, Beijing 100084, China, [3]Department of Chemistry, Brown University, Providence, Rhode Island 02912, USA, [4]Department of Chemistry, Fudan University, Shanghai 200433, China. *e-mail: junli@tsinghua.edu.cn (J.L.); lisidian@sxu.edu.cn (S-D.L.); Lai-Sheng_Wang@brown.edu (L-S.W.)

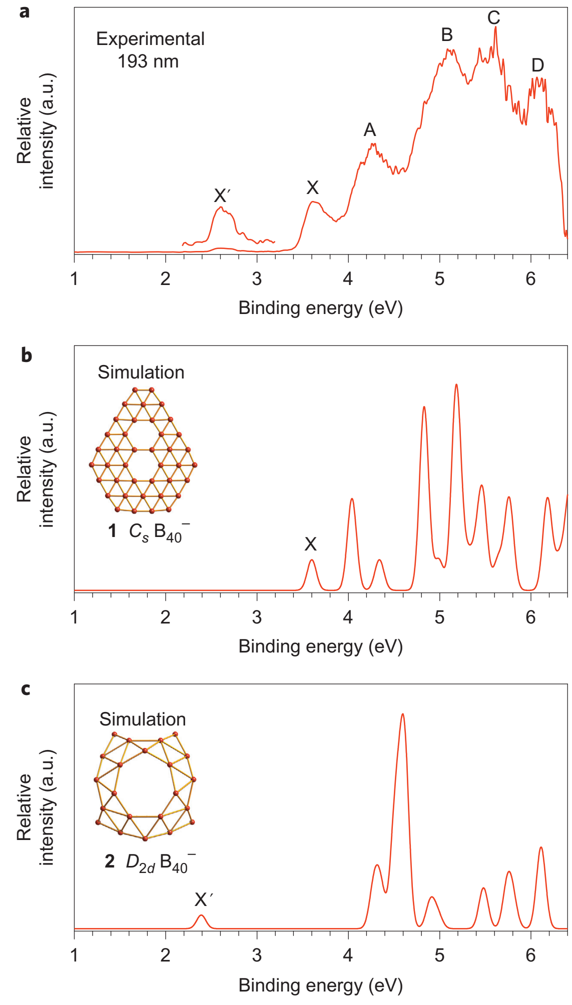

Figure 1 | Photoelectron spectrum of the B_{40}^- cluster and comparison with simulated spectra. **a**, Experimental spectrum at 193 nm (6.424 eV) detachment photon energy. The inset for the weak band X′ at ~2.6 eV binding energy is magnified eight times to show the details. The labels X′, X, A, B, C and D denote observed photodetachment transitions from the B_{40}^- anion to the final electronic states of neutral B_{40}. The X′ band represents an isomer of B_{40}^- with an extremely low electron-binding energy compared with those of all known boron clusters, which suggests a cluster with an unusual structure. **b**, Simulated spectrum at the PBE0 level, based on the quasi-planar structure **1** (C_s, $^2A'$). The major experimental bands (X, A, B, C and D) are well reproduced by the simulated spectrum. **c**, Simulated spectrum based on the cage-like fullerene structure **2** (D_{2d}, $^2B_2$) that shows the large energy gap between the first and second bands. Band X′ with a low binding energy is well reproduced by the D_{2d} cage structure and no planar structures would yield such a feature of low binding energy. The simulations were done by fitting the distributions of calculated vertical detachment energies at the PBE0 level with unit-area Gaussian functions of 0.1 eV half-width. a.u., arbitrary units.

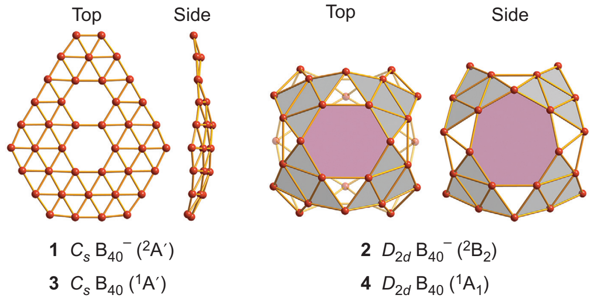

Figure 2 | Top and side views of the global minimum and low-lying isomers of B_{40}^- and B_{40} at the PBE0/6-311+G* level. The simulated photoelectron spectra from the anionic species of these two structures are compared with the experimental data in Fig. 1. **1** (C_s) is the quasi-planar global minimum and **2** (D_{2d}) is the nearly degenerate low-lying fullerene-like cage structure of the negatively charged B_{40}^-. **3** (C_s) is the low-lying isomer and **4** (D_{2d}) is the global minimum of the neutral B_{40}. There is very little structural change between the anion and the neutral cluster in each isomer. Detailed structural parameters for both the anions and the neutrals are given in Supplementary Table 1. The symbols in parentheses represent the spectroscopic states of each species. The hexagonal face of the top view of the cage structure is shaded in purple, along with four B_6 triangles shaded in grey. The bottom half of the B_{40} cage is identical with the top half, but rotated by 90°. In the side view of the cage structure, the heptagonal face is shaded in purple along with four B_6 triangles shaded in grey. There are two hexagonal and four heptagonal faces on the cage surface.

PBE0 geometries and a 6-31G* basis set were performed for the two lowest isomers. All the DFT levels of theory predict the quasi-planar global-minimum structure **1** (C_s, $^2A'$) for B_{40}^- along with the low-lying cage-like fullerene structure **2** (D_{2d}, $^2B_2$), within ~2 kcal mol^{-1} at the PBE0 level (Fig. 2). The CCSD calculations show that structure **2** is 1.7 kcal mol^{-1} higher in energy than structure **1**, consistent with the DFT results.

A configurational energy spectrum of B_{40}^- at the PBE0 level is shown in Fig. 3a, in which representative structures (quasi-planar, cage-like, double-ring and triple-ring isomers) are depicted according to their relative energies. The potential energy surface of B_{40}^- is relatively rugged, with ten low-lying structures located within ~1 eV above the global minimum, which are either quasi-planar or cage-like. The double-ring and triple-ring structures are much higher in energy (Fig. 3a). For the neutral B_{40} cluster (Fig. 3b), the cage structure **4** (D_{2d}, $^1A_1$) becomes well separated from other isomers and clearly defines the global minimum. The next three isomers also possess cage-like structures (positional isomers of structure **4**), being at least ~0.5 eV higher in energy at the PBE0 level, and the nearest quasi-planar isomer **3** (C_s, $^1A'$), which corresponds to the anion global minimum, is ~1.0 eV higher in energy (Fig. 3b). Apparently, the B_{40}^- cluster favours slightly the quasi-planar geometry, whereas the B_{40} neutral cluster favours overwhelmingly the cage-like structures.

Comparison of the experimental and computational data. To confirm the global minimum and low-lying structures of B_{40}^-, we calculated their ADEs and VDEs using the time-dependent DFT (TDDFT) formalism[35]. The simulated spectra for **1** and **2** are compared with the experimental spectrum in Fig. 1. Clearly, neither structure **1** nor structure **2** can reproduce the observed spectrum. However, their combination is in excellent agreement with the experimental data. Structure **1** gives a ground-state ADE/VDE of 3.51/3.60 eV at the PBE0 level, consistent with the experimental data of 3.51/3.63 eV for the X band. Higher binding-energy transitions from structure **1** also agree well with the observed spectral bands A–D, which each clearly contain multiple detachment channels.

However, the calculated ground-state ADE/VDE from structure **2** is 2.39/2.39 eV at the PBE0 level, in close agreement with band X′ (ADE/VDE, 2.50/2.62 eV). As a result of the overlap of the higher binding-energy transitions from **2** with those of **1**, detailed assignments are not feasible. Even so, contributions of structure **2** are expected to be minor because of its slightly higher energy. Additional simulations at the TPSSh, B3LYP and PBE levels produce similar spectral patterns (Supplementary Fig. 4). Interestingly, all four lowest-lying cage-like B_{40}^- isomers (positional isomers of **2**) give rise to a low first VDE close to 2.6 eV, and all four lowest-lying quasi-planar isomers give much higher first VDEs close

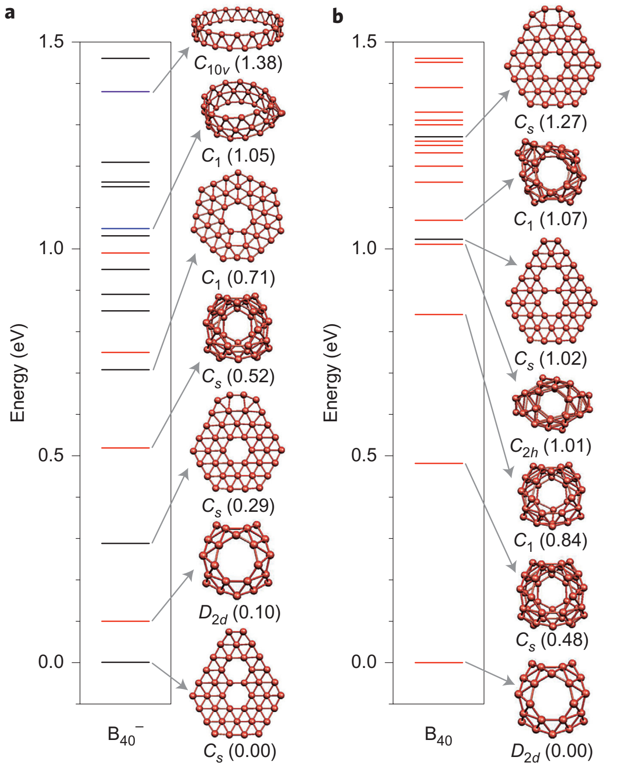

Figure 3 | Configurational energy spectra at the PBE0/6-311+G* level. **a**, B_{40}^-. **b**, B_{40}. The energies of the global minima are taken to be zero. More detailed isomer populations are given in Supplementary Figs 2 and 3 for B_{40}^- and B_{40}, respectively, as well as energetic information calculated at different levels of theory. Black, quasi-planar structures; red, fullerene-like cages; violet, double-ring tubular structures; blue, triple-ring tubular structure.

to 3.6 eV (Supplementary Fig. 5), which lends further support to the coexisting cage-like and quasi-planar isomers being responsible for the observed photoelectron spectra of B_{40}^-.

Discussion

The first all-boron fullerenes. The experimental observation of structure **2** of B_{40}^- represents the first all-boron fullerene ever produced and characterized, even though boron cages have been speculated and explored computationally[15–27]. Both structure **2** and its neutral form **4** have D_{2d} symmetry, with 16 tetracoordinated and 24 pentacoordinated boron atoms. The all-boron fullerenes **2** and **4** are elongated slightly along the two-fold main molecular axis, with two hexagonal holes at the top and bottom and four heptagonal holes on the waist (shaded purple in Fig. 2). These structures are akin to a perforated Chinese red lantern, with two convex caps oriented perpendicularly and supported by four double-chain ribs. The all-boron fullerenes are made of interwoven double-chain boron ribbons that consist of eight horizontal B_9 ribbons and four vertical B_{10} ribbons. Alternatively, the B_{40} cage can be built from eight equivalent, almost perfectly planar, close-packed B_6 triangles (grey-shaded in Fig. 2) that share four corners within the top half of the cage and four within the bottom half. The all-boron fullerenes follow Euler's rule, which in this case reads: E (92 edges) = F (48 triangular + 2 hexagonal + 4 heptagonal faces) + V (40 vertices) − 2. The heptagonal holes observed in **2** and **4** are not known in boron clusters or any previously proposed boron nanostructures.

Although it has been suggested that heptagons are responsible for negative curvatures in carbon nanotubes[36], they have not been observed in any pristine fullerenes. The carbon atoms assume sp^2 hybridization in fullerenes (pentagons and hexagons made up of the fullerene surfaces present the least strain). However, a number of halogenated fullerenes have been synthesized and shown to contain a heptagon[37]. The heptagon seems to release the strains caused by sp^3 carbons present in the halogenated fullerenes, as reflected by the fact that the heptagons in these fullerenes are not perfectly flat. As seen in Fig. 2 (**2** and **4**), the surface of the B_{40} cage is not perfectly smooth—the heptagons may play similar roles as in the heptafullerenes in terms of strain reduction, which results in its overwhelming stability.

To provide further insight into the stability of the B_{40} fullerene, we compared its cohesive energy at the PBE0 level of theory with those of other neutral boron clusters that have been characterized previously (Supplementary Fig. 6). As expected, the cohesive energies of the 2D boron clusters increase monotonically with the cluster size from B_7 to B_{40}. Interestingly, low-lying cage-like structures start to emerge at B_{32}. The cage isomers for B_{32} and B_{36} are less stable than their respective 2D structures by 0.028 eV per atom and 0.081 eV per atom, respectively. The crossover is estimated to be at B_{38}. The B_{40} fullerene is overwhelmingly more stable than the 2D structure, even though, for the B_{40}^- anion, the 2D structure is slightly more stable than the fullerene form. As is shown below, the unfavourable stability of the B_{40}^- fullerene is a direct result of the large HOMO–LUMO gap, which is reflected in the stability of the neutral B_{40} cage.

Molecular dynamics simulations for the B_{40} fullerene show that it is highly robust even at high temperatures, and dynamically stable at 700 and 1,000 K for the 30 ps duration used in the simulation (Supplementary Fig. 7). We also found that the B_{40} fullerene possesses three-dimensional (3D) aromaticity with calculated nucleus-independent chemical shifts[38] of −43 and −42 ppm at the cage centres for **2** and **4**, respectively.

Chemical bonding in the all-boron fullerenes. The exceptional stability of the neutral B_{40} fullerene is also evident by the large energy gap, as shown in the simulated spectrum (Fig. 1c). Owing to the overlap of the higher binding-energy features of **2** with those of **1**, we could not obtain the experimental energy gap for **2**. Our calculation gave a very large HOMO–LUMO gap of 3.13 eV (Supplementary Fig. 8) for the neutral cage **4** at the PBE0 level, which is comparable to that of C_{60} (3.02 eV) calculated at the same level. Supplementary Fig. 8 shows that the LUMO of **4** is a non-degenerate b_2 orbital in which the extra electron resides in the B_{40}^- cage; this explains why both **2** and **4** can have the same D_{2d} symmetry without symmetry breaking when an electron is added or detached. On the one hand, the large HOMO–LUMO gap of **4** underlies the overwhelmingly high stability of the neutral B_{40} fullerene; at the same time, this large HOMO–LUMO gap is directly responsible for the relatively less-stable B_{40}^- fullerene because the extra electron has to occupy the high-energy LUMO in the anion. On the other hand, the C_s 2D isomer of B_{40} (**3** in Fig. 2) has a very small HOMO–LUMO gap (Fig. 1b). In fact, the difference in the HOMO–LUMO gaps of **3** and **4** reflects almost exactly the difference in stability of the 2D and cage structures in the anion.

We analysed the bonding in the closed-shell neutral fullerene **4** using adaptive natural density partitioning (AdNDP)[39]. Of the 60 pairs of valence electrons in **4**, a total of 48 delocalized σ bonds were readily identified (Fig. 4): 40 three-centre two-electron (3c–2e) σ bonds on the B_3 triangles and eight 6c–2e σ bonds on the quasi-planar close-packed B_6 units. As the central B_3 triangles make major contributions to the 6c–2e σ bonds, the 48 σ bonds can all be viewed practically as 3c–2e bonds, which match exactly the number of B_3 triangles on the surface of **4**, completely and uniformly distributed over the cluster surface, one on each B_3

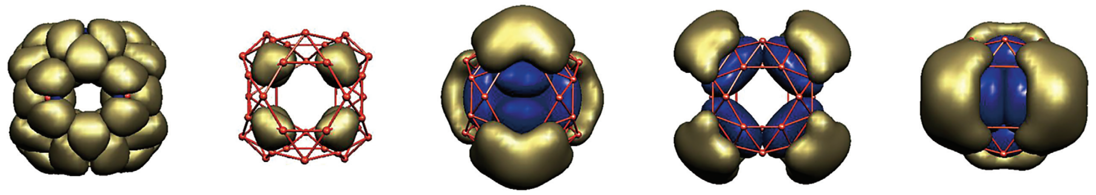

40 × 3c−2e σ bonds ON = 1.87–1.96 |e|

8 × 6c−2e σ bonds ON = 1.91 |e|

4 × 5c−2e π bonds ON = 1.95 |e|

4 × 6c−2e π bonds ON = 1.96 |e|

4 × 7c−2e π bonds ON = 1.93 |e|

Figure 4 | Results of chemical bonding analyses for the B_{40} fullerene. The analyses were done using the AdNDP method[39]. Each lobe in the five frames represents a multicentre two-electron bond, with the occupation number (ON) given below each frame. There are 40 three-centre two-electron σ bonds, given as 40 × 3c–2e σ bonds, and eight six-centre two-electron σ bonds (8 × 6c–2e σ bonds). The eight six-centre σ bonds are localized mainly on the central B_3 triangle of each grey-shaded B_6 triangle in **4** (Fig. 2). Hence, there is essentially one 3c–2e delocalized σ bond for each of the 48 triangular faces of the B_{40} cage. The π bonds are classified using the cage surface as the nodal plane. There are 12 delocalized multicentre two-electron π bonds along the interwoven double-boron chains, including four five-centre, four six-centre and four seven-centre π bonds. All the 120 valence electrons of the B_{40} cage form delocalized bonds (48 σ and 12 π bonds) uniformly over the surface of the cage without any classical two-centre two-electron localized bonds. This bonding pattern of the all-boron B_{40} fullerene cage is extraordinary and unprecedented among all known boron clusters.

triangle. The remaining 12 bonds in **4** can be characterized essentially as delocalized π bonds: four 5c–2e π bonds, four 6c–2e π bonds and four 7c–2e π bonds distributed evenly over the cage surface along the interwoven double-boron chains. Thus, all the valence electrons in **4** are either delocalized σ or π bonds and there is no localized 2c–2e bond, unlike the 2D boron clusters[4–8,10,11]. According to our AdNDP analysis, on average each boron atom contributes 0.6 electrons to the π framework. The completely delocalized σ and π bonding in the B_{40} fullerene is unprecedented, and is the underlying reason for its exceptional stability.

On the concentric dual π aromaticity in the quasi-planar isomer. The quasi-planar B_{40}^- isomer **1** (C_s, $^2A'$) is also extremely interesting. The 2D-to-3D crossover occurs at B_{16}^+ for cationic boron clusters[9], but it is still unresolved for neutral boron clusters[40]. The B_n^- anionic clusters are known to adopt 2D structures up to at least $n = 24$ (ref. 8) and remain 2D at $n = 36$ (ref. 11). The current results suggest that the critical size for the 2D-to-3D crossover of the anionic boron clusters is probably around $n = 40$. The stability and planarity of **1** may be understood on the basis of its concentric dual π aromaticity, analogous to the planar hydrocarbon $C_{27}H_{13}^+$ (Supplementary Fig. 9). The π-bonding pattern based on the AdNDP analysis of the closed-shell doubly charged **1** is almost identical to that of the model $C_{27}H_{13}^+$ unsaturated hydrocarbon, as shown in Supplementary Fig. 10. Also, the quasi-planar C_s B_{40}^{2-} dianion appears to be thermodynamically stable in the gas phase, with a calculated ADE of ~0.7 eV at the PBE0 level (Supplementary Fig. 11). It is 1.46 eV more stable than the D_{2d} B_{40}^{2-} fullerene. More interestingly, the two adjacent hexagonal holes in the triangular lattice of **1** are reminiscent of a 2D boron β sheet[13]. If B_{36} can be viewed as the embryo of the boron α sheet[11], then different types of β sheets[41] may be constructed from isomer **1** or **3**, which suggests the viability of extended boron β sheets (or α and β binary sheets), that is, different types of borophene.

Conclusion

As a result of the electron deficiency of boron, strong covalent interactions are anticipated between neighbouring fullerene B_{40} units in the condensed phase, which makes it difficult to form B_{40}-based materials, such as a fullerite analogue[42], with the B_{40} cage as isolated building blocks. However, chemical modification and functionalization of the B_{40} fullerene should be possible. Initial calculations indicate that doping **4** with a metal atom M (= Ca, Y, La) results in endohedral boron fullerenes M@B_{40} with M slightly off-centre along the two-fold molecular axis, analogous to Ca@C_{60} (ref. 43). In fact, as all-boron fullerenes **2** and **4** possess a slightly smaller diameter (6.2 Å relative to 7.1 Å for C_{60}), they can accommodate more comfortably an endohedral atom than can C_{60}. Preliminary calculations also suggest that **2** and **4** offer valuable model systems for hydrogen storage. For example, an H_2 molecule can be activated in an encapsulated $H_2@B_{40}^{-/0}$ and up to 16 hydrogen atoms can be bonded terminally at the 16 tetracoordinate boron sites of **2** and **4**. In particular, Ca-coated B_{40} may serve as a promising material for H_2 chemisorption[44]. Notably, every boron atom in **2** and **4** is on the edge of a hexagonal or heptagonal hole, which may facilitate H and/or H_2 adsorption and release. Only a handful of free-standing elemental cage clusters have been characterized experimentally thus far[1,45–47]: the fullerenes, Au_{16}^-, stannaspherene Sn_{12}^{2-} and plumbaspherene Pb_{12}^{2-}. The observation of the all-boron fullerene, for which we propose the name "borospherene", enriches the chemistry of boron and may lead to new boron-based nanomaterials.

Methods

Photoelectron spectroscopy. The experiment was carried out using a magnetic-bottle PES apparatus[28] equipped with a laser vaporization cluster source. Briefly, the B_{40}^- clusters were produced using a ^{10}B-enriched boron disc target in the presence of a helium carrier gas seeded with 5% Ar and were mass selected using a time-of-flight mass spectrometer. Photodetachment experiments were conducted with a magnetic-bottle electron analyser at two photon energies: 193 nm (6.424 eV) and 266 nm (4.661 eV). The photoelectron spectra were calibrated using the known spectra of Au^- and Rh^-. The energy resolution of the apparatus was $\Delta E/E \approx 2.5\%$, that is, ~25 meV for 1 eV kinetic energy electrons.

Computational methods. The stochastic surface walking (SSW) structural searches[29] of the potential energy surfaces of B_{40}^- were conducted from 16 independent SSW runs from randomly distributed atoms in a spherical box. In total, 3,027 minima were evaluated and the D_{2d} fullerene was found to be the global minimum. To confirm the stability of the global minimum, another 40 SSW runs were conducted, starting from the D_{2d} structure, and no structure of lower energy was found within a total of 3,565 minima. Similarly, for the C_s planar clusters obtained through a number of guess structures, we also conducted 24 independent SSW runs to confirm its stability, each starting from the C_s structure. These two minima are located at two well-separated funnels on the potential energy surfaces and it is not feasible to interconvert these structures within the current timescale of SSW searches. Independently, the TGmin program developed at Tsinghua University was employed to search for the global minimum of B_{40}^-. The TGmin program, used previously to search for the global minimum of B_{36}^- (ref. 11), is based on the basin hopping (BH) algorithm[30], but with many constraints implemented so as to reduce the size of the search space. Both planar and non-planar B_{40}^- anion clusters were searched, amounting to more than 5,300 structures, which included the D_{2d} fullerene-like structure. Similar global-minimum searches were performed for neutral B_{40} using the SSW and TGmin approaches. All low-lying structures were subsequently optimized at the PBE, PBE0 and TPSSh levels with the 6-311+G* basis set. The CCSD/6-31G* single-point energy calculations were carried out using NWCHEM 6.3 to obtain more-accurate relative energies[48]. The ground-state ADEs and VDEs were calculated at the DFT levels. The VDEs for the excited states and the simulated spectra were obtained using TDDFT methods. All electronic structure calculations were performed using the Gaussian 09 package[49], whereas the CCSD calculations were performed with NWCHEM and MOLPRO[50].

Received 11 February 2014; accepted 9 June 2014;
published online 13 July 2014

References

1. Kroto, H. W. *et al.* C_{60}: buckminsterfullerene. *Nature* **318,** 162–163 (1985).
2. Research highlight: new balls, please. *Nature* **447,** 4 (2007).
3. La Placa, S. J., Roland, P. A. & Wynne, J. J. Boron clusters (B_n, $n = 2–52$) produced by laser ablation of hexagonal boron nitride. *Chem. Phys. Lett.* **190,** 163–168 (1992).
4. Zhai, H. J. *et al.* Hepta- and octa-coordinate boron in molecular wheels of eight- and nine-atom boron clusters. *Angew. Chem. Int. Ed.* **42,** 6004–6008 (2003).
5. Zhai, H. J. *et al.* Hydrocarbon analogues of boron clusters – planarity, aromaticity, and antiaromaticity. *Nature Mater.* **2,** 827–833 (2003).
6. Kiran, B. *et al.* Planar-to-tubular structural transition in boron clusters: B_{20} as the embryo of single-walled boron nanotubes. *Proc. Natl Acad. Sci. USA* **102,** 961–964 (2005).
7. Huang, W. *et al.* A concentric planar doubly π-aromatic B_{19}^- cluster. *Nature Chem.* **2,** 202–206 (2010).
8. Popov, I. A. *et al.* A combined photoelectron spectroscopy and *ab initio* study of the quasi-planar B_{24}^- cluster. *J. Chem. Phys.* **139,** 144307 (2013).
9. Oger, E. *et al.* Boron cluster cations: transition from planar to cylindrical structures. *Angew. Chem. Int. Ed.* **46,** 8503–8506 (2007).
10. Sergeeva, A. P. *et al.* Understanding boron through size-selected clusters: structure, chemical bonding, and fluxionality. *Acc. Chem. Res.* **47,** 1349–1358 (2014).
11. Piazza, Z. A. *et al.* Planar hexagonal B_{36} as a potential basis for extended single-atom layer boron sheets. *Nature Commun.* **5,** 3113 (2014).
12. Quandt, A. & Boustani, I. Boron nanotubes. *Chem. Phys. Chem.* **6,** 2001–2008 (2005).
13. Tang, H. & Ismail-Beigi, S. Novel precursors for boron nanotubes: the competition of two-center and three-center bonding in boron sheets. *Phys. Rev. Lett.* **99,** 115501 (2007).
14. Yang, X. B., Ding, Y. & Ni, J. *Ab initio* prediction of stable boron sheets and boron nanotubes: structure, stability, and electronic properties. *Phys. Rev. B* **77,** 041402(R) (2008).
15. Szwacki, N. G., Sadrzadeh, A. & Yakobson, B. I. B_{80} fullerene: an *ab initio* prediction of geometry, stability, and electronic structure. *Phys. Rev. Lett.* **98,** 166804 (2007); erratum **100**, 159901 (2008).
16. Yan, Q. B. *et al.* Family of boron fullerenes: general constructing schemes, electron counting rule, and *ab initio* calculations. *Phys. Rev. B* **78,** 201401 (2008).
17. Zope, R. R. *et al.* Boron fullerenes: from B_{80} to hole doped boron sheets. *Phys. Rev. B* **79,** 161403 (2009).
18. Sheng, X. L., Yan, Q. B., Zheng, Q. R. & Su, G. Boron fullerenes B_{32+8k} with four-membered rings and B_{32} solid phases: geometrical structures and electronic properties. *Phys. Chem. Chem. Phys.* **11,** 9696–9702 (2009).
19. Ozdogan, C. *et al.* The unusually stable B_{100} fullerene, structural transitions in boron nanostructures, and a comparative study of α- and γ-boron and sheets. *J. Phys. Chem. C* **114,** 4362–4375 (2010).
20. Wang, L. *et al.* Boron fullerenes with 32–56 atoms: irregular cage configurations and electronic properties. *Chem. Phys. Lett.* **501,** 16–19 (2010).
21. Muya, J. T., Gopakumar, G., Nguyen, M. T. & Ceulemans, A. The leapfrog principle for boron fullerenes: a theoretical study of structures and stability of B_{112}. *Phys. Chem. Chem. Phys.* **13,** 7524–7533 (2011).
22. Zope, R. R. & Baruah, T. Snub boron nanostructures: chiral fullerenes, nanotubes and planar sheet. *Chem. Phys. Lett.* **501,** 193–196 (2011).
23. Polad, S. & Ozay, M. A new hole density as a stability measure for boron fullerenes. *Phys. Chem. Chem. Phys.* **15,** 19819–19824 (2013).
24. Prasad, D. L. V. K. & Jemmis, E. D. Stuffing improves the stability of fullerenelike boron clusters. *Phys. Rev. Lett.* **100,** 165504 (2008).
25. De, S. *et al.* Energy landscape of fullerene materials: a comparison of boron to boron nitride and carbon. *Phys. Rev. Lett.* **106,** 225502 (2011).
26. Li, F. Y. *et al.* B_{80} and $B_{101–103}$ clusters: remarkable stability of the core–shell structures established by validated density functionals. *J. Chem. Phys.* **136,** 074302 (2012).
27. Boulanger, P. *et al.* Selecting boron fullerenes by cage-doping mechanisms. *J. Chem. Phys.* **138,** 184302 (2013).
28. Wang, L. S., Cheng, H. S. & Fan, J. Photoelectron spectroscopy of size-selected transition metal clusters: Fe_n^-, $n = 3–24$. *J. Chem. Phys.* **102,** 9480–9493 (1995).
29. Shang, C. & Liu, Z. P. Stochastic surface walking method for structure prediction and pathway searching. *J. Chem. Theory Comput.* **9,** 1838–1845 (2013).
30. Wales, D. J. & Scheraga, H. A. Global optimization of clusters, crystals, and biomolecules. *Science* **285,** 1368–1372 (1999).
31. Krishnan, R., Binkley, J. S., Seeger, R. & Pople, J. A. Self-consistent molecular orbital methods. XX. A basis set for correlated wave functions. *J. Chem. Phys.* **72,** 650–654 (1980).
32. Perdew, J. P., Burke, K. & Ernzehof, M. Generalized gradient approximation made simple. *Phys. Rev. Lett.* **77,** 3865–3868 (1996).
33. Adamo, C. & Barone, V. Toward reliable density functional methods without adjustable parameters: the PBE0 model. *J. Chem. Phys.* **110,** 6158–6165 (1999).
34. Tao, J., Perdew, J. P., Staroverov, V. N. & Scuseria, G. E. Climbing the density functional ladder: nonempirical meta-generalized gradient approximation designed for molecules and solids. *Phys. Rev. Lett.* **91,** 146401 (2003).
35. Bauernschmitt, R. & Ahlrichs, R. Treatment of electronic excitations within the adiabatic approximation of time dependent density functional theory. *Chem. Phys. Lett.* **256,** 454–464 (1996).
36. Iijima, S., Ichihashi, T. & Ando, Y. Pentagons, heptagons, and negative curvature in graphite microtubule growth. *Nature* **356,** 776–778 (1992).
37. Troshin, P. A. *et al.* Isolation of two seven-membered ring C_{58} fullerene derivatives: $C_{58}F_{17}CF_3$ and $C_{58}F_{18}$. *Science* **309,** 278–281 (2005).
38. Schleyer, P. v. R. *et al.* Nucleus-independent chemical shifts: a simple and efficient aromaticity probe. *J. Am. Chem. Soc.* **118,** 6317–6318 (1996).
39. Zubarev, D. Y. & Boldyrev, A. I. Developing paradigms of chemical bonding: adaptive natural density partitioning. *Phys. Chem. Chem. Phys.* **10,** 5207–5217 (2008).
40. Romanescu, C., Harding, D. J., Fielicke, A. & Wang, L. S. Probing the structures of neutral boron clusters using infrared/vacuum ultraviolet two-color ionization: B_{11}, B_{16}, and B_{17}. *J. Chem. Phys.* **137,** 014317 (2012).
41. Penev, E. S., Bhowmick, S., Sadrzadeh, A & Yakobson, B. I. Polymorphism of two-dimensional boron. *Nano Lett.* **12,** 2441–2445 (2012).
42. Kratschmer, W., Lamb, L. D., Fostiropoulos, K. & Huffman, D. R. Solid C_{60}: a new form of carbon. *Nature* **347,** 354–358 (1990).
43. Wang, L. S. *et al.* The electronic structure of $Ca@C_{60}$. *Chem. Phys. Lett.* **207,** 354–359 (1993).
44. Li, M. *et al.* Ca-coated boron fullerenes and nanotubes as superior hydrogen storage materials. *Nano Lett.* **9,** 1944–1948 (2009).
45. Bulusu, S. *et al.* Evidence of hollow golden cages. *Proc. Natl Acad. Sci. USA* **103,** 8326–8330 (2006).
46. Cui, L. F. *et al.* Sn_{12}^{2-}: stannaspherene. *J. Am. Chem. Soc.* **128,** 8390–8391 (2006).
47. Cui, L. F. *et al.* Pb_{12}^{2-}: plumbaspherene. *J. Phys. Chem. A* **110,** 10169–10172 (2006).
48. Valiev, M. *et al.* NWChem: a comprehensive and scalable open-source solution for large scale molecular simulations. *Comput. Phys. Commun.* **181,** 1477–1489 (2010).
49. Frisch, M. J. *et al.* GAUSSIAN 09, Revision A.2 (Gaussian Inc., Wallingford, Connecticut, 2009).
50. Werner, H. J. *et al.* MOLPRO, version 2012.1 (www.molpro.net).

Acknowledgements

This work was supported by the US National Science Foundation (CHE-1263745 to L-S. W.), the National Natural Science Foundation of China (20825311, 21173051, 21243004 and 21373130), the National Key Basic Research Special Foundations (2011CB808500, 2013CB834603 and 2011CB932401), the Shanxi International Cooperation project (2013081018) and the Science and Technology Commission of Shanghai Municipality (08DZ2270500). H-J.Z. gratefully acknowledges the support of a start-up fund from Shanxi University. The calculations were performed using supercomputers at the Computer Network Information Center, Chinese Academy of Sciences and Tsinghua National Laboratory for Information Science and Technology.

Author contributions

H-J.Z., S-D.L., J.L. and L-S.W. designed the project. H-J.Z. and W-L.L. carried out the experiments. Q.C., H.B., W-J.T., H-G.L., Y-B.W. and Y-W.M. constructed the guess structures and did the electronic structure calculations and spectral simulations. G-F.W., Z-P.L. and Y-F.Z. did the SSW and BH structural searches independently. H-S.H. performed the CCSD calculations. H-J.Z., J.L., S-D.L. and L-S.W. analysed the data and wrote the paper. All authors discussed the results and made comments and edits to the manuscript.

Additional information

Supplementary information is available in the online version of the paper. Reprints and permissions information is available online at www.nature.com/reprints. Correspondence and requests for materials should be addressed to J.L., S.D.L. and L.S.W.

Competing financial interests

The authors declare no competing financial interests.